Isoxazole analogues bind the System x_c^- transporter: Structure–activity relationship and pharmacophore model

Sarjubhai A. Patel [a], Trideep Rajale [a,b], Erin O'Brien [a], David J. Burkhart [b,†], Jared K. Nelson [b,‡], Brendan Twamley [b], Alex Blumenfeld [b], Monika I. Szabon-Watola [a,b], John M. Gerdes [a], Richard J. Bridges [a], Nicholas R. Natale [a,b,*]

[a] NIH COBRE Center for Structural and Functional Neuroscience, The University of Montana, Missoula, MT 59812, USA
[b] Department of Chemistry University of Idaho, Moscow, ID 83844-2343, USA

ABSTRACT

Analogues of amino methylisoxazole propionic acid (AMPA), were prepared from a common intermediate **12**, including lipophilic analogues using lateral metalation and electrophilic quenching, and were evaluated at System x_c^-. Both the 5-naphthylethyl-(**16**) and 5-naphthylmethoxymethyl-(**17**) analogues adopt an *E*-conformation in the solid state, yet while the former has robust binding at System x_c^-, the latter is virtually devoid of activity. The most potent analogues were amino acid naphthyl-ACPA **7g**, and hydrazone carboxylic acid, **11e** Y = Y′ = 3,5-$(CF_3)_2$, which both inhibited glutamate uptake by the System x_c^- transporter with comparable potency to the endogenous substrate cystine, whereas in contrast the closed isoxazolo[3,4-*d*] pyridazinones **13** have significantly lower activity. A preliminary pharmacophore model has been constructed to provide insight into the analogue structure–activity relationships.

© 2009 Elsevier Ltd. All rights reserved.

1. Introduction

L-Glutamate (L-Glu, **1**, Chart 1) is the primary excitatory neurotransmitter in the mammalian CNS. Through its activation of a wide variety of ionotropic (iGluRs) and metabotropic (mGluRs) excitatory amino acid (EAA) receptors, L-glutamate-mediated signaling contributes to fast synaptic neurotransmission, higher order signal processing (e.g., synaptic plasticity, development, learning and memory), and even to neuropathology.[1] Concentrations of L-Glu in the CNS are regulated by a family of excitatory amino acid transporters (EAATs) that rapidly sequester and concentrate this dicarboxylic amino acid in glia and neurons, and thereby limit its extracellular accumulation and access to EAA receptors. In contrast to the EAAT-mediated uptake of L-Glu, the System x_c^- (Sx_c^-) transporter has been implicated in the export of L-Glu from CNS cells in a manner that allows it to activate EAA receptors. Sx_c^- is a member of the heteromeric amino acid transporter family (HATs; *a.k.a.* glycoprotein-associated amino acid exchangers) that functions as an obligate exchanger. Under physiological conditions Sx_c^- employs the L-Glu concentration

gradient generated by the EAATs as the driving force for the import of L-cystine (L-Cys$_2$, **2**). Thus, the transporter mediates the uptake of a vital sulfur-containing amino acid needed for the synthesis of glutathione (GSH) and oxidative protection,[2] while simultaneously producing an efflux of L-Glu that has the potential to contribute to either excitatory signaling or excitotoxic pathology. The significance of these actions is reflected in the range of CNS processes, to which Sx_c^- has been linked, including: drug addiction,[3,4] brain tumor growth,[5] oxidative protection,[6] viral pathology,[7] the operation of the blood brain barrier,[8] neurotransmitter release,[9] and synaptic organization.[10]

Initial pharmacological studies on Sx_c^- established L-Cys$_2$ and L-Glu as substrates, verified it operated as an obligate exchanger, and defined key features of its specificity, for example: (i) L-aspartate is neither a substrate nor inhibitor, (ii) L-homocysteate is an inhibitor, (i.e., a SO_3^- can replace a distal COO^-) and (iii) L-α-aminoadipate and L-α-aminopimelate are inhibitors (i.e., longer chain lengths are tolerated).[11] Using CNS-derived tumor cell lines that express high levels of Sx_c^-, we have begun to more thoroughly investigate the SAR's governing binding and translocation.[12,13] In addition to the SO_3^- moieties (*S*-sulfo-L-CySH, L-serine-*O*-SO$_3^-$) the binding site also accommodates SO_2^- groups (L-homocysteine-sulfinate), but not the PO_3^{-2} group of L-serine-*O*-PO$_3^{-2}$. The ability to bind higher homologues of L-Glu is substantiated by the actions of *S*-carboxymethyl- and *S*-carboxy-
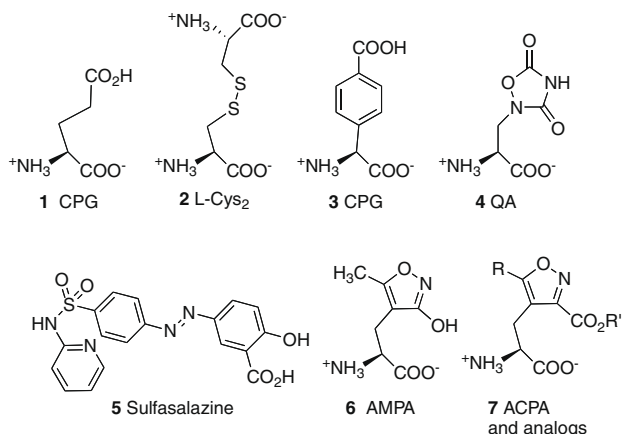
Chart 1. Ligand structures which bind the System x_c^- transporter.

ethyl-L-cysteine. However, there is a limit to this trend, as L-homocystine and L-djenkolate exhibit reduced activities.[12] Several conformationally constrained analogues of Glu also inhibit Sx_c^-, including quisqualate (QA, **4**), 4-S-carboxy-phenylglycine (4-S-CPG), ibotenate (IBO), (RS)-4-Br-homoibotenate, and (RS)-5-Br-willardiine.[12,14,15] Interestingly, several of these latter analogues are much better known for activities at other iGluRs and mGluRs, where the conformationally restricted positioning of their functional groups have presumably increased their specificity of action, as well as added to their value in delineating the respective binding site pharmacophores for the various receptors. Among these analogues, the actions of natural products QA and IBO as Sx_c^- inhibitors highlighted the potential use of isoxazoles as a scaffold for the development of additional blockers for this transporter. One of the best known of the isoxazoles is amino-methyl isoxazole propionic acid (**6**, AMPA),[16] which was the defining agonist for the GluR1-4 receptor subtypes (a.k.a. AMPA receptors).[1] While AMPA itself exhibits little or no activity at Sx_c^-, we have begun to explore the potential inhibitory activity of other AMPA analogues that have emerged from the pioneering studies of Krogsgaard-Larsen and co-workers.[17] In this work a series of amino-3-carboxy-5-methylisoxazole propionic acid (ACPA) analogues is evaluated for inhibitory activity at Sx_c^-. Interestingly, we find that the introduction of lipophilic groups to the ACPA base structure, as exemplified by **7**, provides a point of divergence that distinguishes the binding sites of GluR2 and Sx_c^-. This, in turn led us to examine non-amino acid bioisosteres of ACPA, and we have found that several hydrazone acids (**11** and **16**, Chart 2) bind to the Sx_c^- with affinities comparable to those of the endogenous substrates. In contrast, the isoxazolo[3,4-d] analogues **13** exhibit little or no binding to this transporter. These novel isoxazole-based analogues are used in combination with SAR data from other structurally diverse inhibitors (e.g., 4-S-CPG, sulfasalazine (**5**)) to construct a pharmacophore model of the Sx_c^- substrate binding site.

2. Results and discussion

2.1. Preparation of amino acid analogues of AMPA

The amino acid analogues of AMPA were prepared using synthetic methodology previously described by our laboratory, with the exception of MOM- and BOM-ACPA, **7b** and **7e**, respectively, which were prepared from the known 5-hydroxymethylene acetal,[18] via a straightforward Williamson ether synthesis, and carried forward to the amino acids using our previously described sequence.[19]

2.2. Chemistry: steric and electronic influence on the preparation of isoxazole–hydrazones verses isoxazolo[3,4-d]pyridazinones

The synthesis of isoxazole–hydrazones proceeds to the open form only if electron withdrawing groups are present on the ring.[20] In our hands, no conditions could be discovered to inhibit the cyclization of aryl containing electron donating groups, and these proceed to the isoxazolo[3,4-d]pyridazinones **13** ([3,4-d]).[21] Variable temperature NMR studies indicate that the E- to Z-conversion begins at elevated temperature (ca. 60 °C) and the ring closure appears to be irreversible. Therefore, to deliberately synthesize the closed [3,4-d] analogues **13** the reactions were conducted at reflux.[22–32] In those cases where the open forms were isolated, the best yields were obtained by conducting the reaction at room temperature, and the subsequent hydrolysis at the lowest temperature practical to effect conversion to the products **11**, **16** and **17** (Scheme 1).

The lipophilic analogues listed are only representative, and prepared using lateral metalation and electrophilic quenching as previously described by our group.[19] After deprotection and hydrazone formation E- and Z-isomers of the esters are almost always observed. We have isolated and crystallized both E-**14a** (Fig. 4A) and Z-**14b** (Fig. 4B), and examined their structures by X-ray crystallography. Complete Crystallographic Information Files (CIF) are contained in the Supplementary data. The Z-form **14b** exhibits an
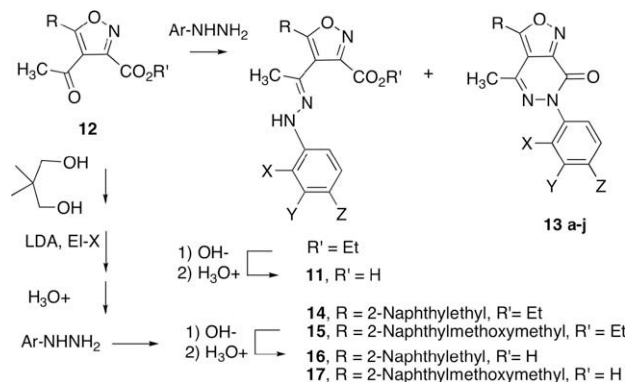
Scheme 1. Analogs of AMPA: open **11**, **16**, **17** and closed isoxazolo[3,4-d]pyridazinones **13**.
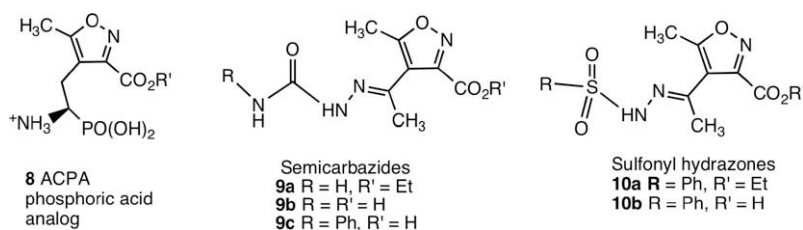

Chart 2. Non-amino acid analogs of AMPA/ACPA.

almost orthogonal relationship between the isoxazole mean plane and C=N hydrazone, and the NH is virtually perfectly poised for cyclization to the [3,4-d] **13**. On hydrolysis, the purified Z-forms convert on standing in solution to the [3,4-d]. Of paramount importance in comparing the biology of open to closed forms is the *caveat* that it was necessary to make the solutions up freshly before study, and to verify after the assay that the open formed was indeed still open, which in some cases (i.e., **11a** to **13a**) occurs in a matter of a few hours. The E-forms of the hydrazone acids with electron withdrawing groups appear to be more conformationally stable.

2.3. Inhibition of uptake of glutamate at the System x_c^- transporter

Inhibitory activity at Sx_c^- was assessed by quantifying the ability of the analogues to attenuate the uptake of L-^{3}H]-Glu into human SNB-19 glioblastoma cells under Cl-dependent (Na-free) conditions. These cells, as well as other glial tumor-derived lines, exhibit much higher levels of Sx_c^- activity than do primary astrocytes and are thus well suited for pharmacological assays.[12,33] Compounds were initially screened at a single concentration (e.g., 250 μM or 500 μM) with Sx_c^- activity reported as a % of control uptake: 573 ± 16 pmol/min/mg protein (mean ± SEM, n = 22). In this respect, lower values denote greater levels of inhibition. As summarized in Table 1, the first series of isoxazoles examined, which included the well-known AMPA receptor ligands AMPA (**6**) and ACPA (**7**), exhibited no discernable activity at Sx_c^-. A similar lack of activity was also observed with phosphonate derivative of ACPA (**8**), as well as those isoxazoles to which small aliphatic groups had been added to C(5), (**7a**–**7c**). In contrast, however, the placement of aromatic functional groups, such as phenethyl (**7d**), benzyloxymethyl (**7e**), and 1- or 2-naphthylethyl (**7f** and **7g**, respectively), at C(5) yielded amino acids with the capacity to markedly inhibit the transporter. The increased inhibitory activity of the compounds suggest that the presence of the larger aromatic moieties enhanced binding to the transporter either by influencing the relative configurations of the functional groups participating in substrate binding or through direct interaction with lipophilic domains adjacent to the substrate site, or both. These structure–activity relationships are also noteworthy in light of the observation that **7d**, **7f** and **7g** exhibit essentially no ability to displace radiolabeled AMPA in brain slice experiments.[34]

This initial group of isoxazoles screened as Sx_c^- inhibitors (Table 1) also included modifications to the free amino group of ACPA, including: semicarbazide hydrazone (**9a** and **9b**), benzene–sufonylhydrazone (**10a** and **10b**), phenylsemicarbazide hydrazone (**9c**), and arylhydrazone (**11e**) bioisosteres. While for the most part inactive, the latter two analogues (**9c** and **11e**) exhibited a moderate amount of inhibitory activity and prompted the synthesis and characterization of the hydrazone derivatives listed in Table 2. These compounds also included the corresponding pyridazones that formed following intramolecular ring closure. In general these bicyclic [3,4-d] analogues (**13a–j**) exhibited little or no activity and in the instances where inhibition was observed, in every case the structurally open parent hydrazones (**11a–f**) were markedly more potent. For example: **11a** produced 44% inhibition compared to 26% for **13a**; **11b** produced 78% inhibition compared to 15% for **13b**; and **11e** produced 86% inhibition compared to 18% for **13j**. While the results indicate that electron withdrawing groups on the aryl moiety appear to correlate with higher levels of Sx_c^- inhibition, this may be the case only because electron donating groups favor select diazene tautomers (Scheme 2) and, thus, encourage cyclization to the less active closed [3,4-d] (**13**). As was observed with modifications at C(5) (Table 1), the presence of lipophilic moieties linked to the amino group also have the potential to increase

the apparent affinity of the ligands. To discern if these lipophilic groups are interacting with distinct transporter domains a hybrid analogue (**16a**) with lipophilic moieties at both C4 and C5 of the isoxazole was prepared. Interestingly, **16a** exhibited the same level of inhibition observed with **11d**, suggesting that the two different aryl groups could be simultaneously accommodated by Sx_c^-. There does appear, however, to be some specificity with regard to these lipophilic domains, as the presence of an additional oxygen in the linkage significantly diminishes activity (i.e., compare **17** with **16a**). More specifically, we previously demonstrated that the corresponding esters of these two acids (**14a** and **15**, respectively)[35] adopt similar E-geometries about the hydrazone moiety, and NMR chemical shifts indicate that this geometry is maintained within the corresponding carboxylic acids **16** and **17**. Worthy of note is that the open hydrazones, such as **8**, **9b**, **9c**, **10b** and **11d** showed no detectable GluR2 binding in Gouaux's S1S2 construct filter assay[36] (Gouaux, personal communication).

Those compounds exhibiting significant levels of inhibition in the initial screening assays were characterized in greater detail by quantifying the concentration-dependence with which the analogues blocked Sx_c^- and calculating corresponding K_i values. These values, which are summarized in Table 3, were determined for most of the blockers using the Cheng–Prusoff equation (i.e., $K_i = (1 + [S]/K_m)/[IC_{50}]$ and IC_{50} values generated from standard inhibition curves (see Fig. 1).[37,38] To confirm that the inhibition could be attributed to a competitive mechanism, a few of the analogues, including the most potent inhibitor (S-2-naphthyl-ethyl-ACPA, **7g**), were also examined using a Michaelis–Menten analysis in which both the concentration of the inhibitor and substrate were systematically varied. A replot of the resulting $K_{m,apparent}$ values versus [I] was then used to determine a K_i value (Fig. 2). Consistent with competitive inhibition, these plots revealed an increase in the apparent K_m without a significant change in V_{max}. A comparison of the K_i values demonstrate that inhibitors **7g**, **11b**, and **11e** each bind to the transporter with an affinity comparable to that of the endogenous substrate L-Cys$_2$, about 50–60 μM. Although all of the inhibitors share an isoxazole structure, the diversity among these ligands also reveals a number of novel properties of the substrate binding site. Thus, **11b** and **11e** stand apart from almost all of the recognized inhibitors of Sx_c^- in that the hydrazone linkage essentially removed the commonly found free α-amino and α-carboxylate groups that typify the amino acids. The aryl groups on these inhibitors, as well as on **7g**, also suggest the presence of lipophilic domains readily adjacent to the substrate binding site that facilitate the binding of the compounds compared to ACPA itself. Further, the fact that hybrid analogue **16a** includes aryl additions at both positions and retains inhibitory activity, suggests that these lipophilic groups are interacting with distinct regions of the protein.

2.4. Substrate activity

While the competition assays discussed above address the specificity of ligand binding, the results provide little insight into whether the analogues are acting as alternative substrates or as non-substrate inhibitors (i.e., compounds that bind but are not translocated) to competitively block uptake. To examine this we have developed an exchange assay in which the substrate-induced efflux of L-Glu is quantified by measuring the conversion of NADP$^+$ to NADPH as the extracellular L-Glu leaves the cells and is rapidly metabolized by glutamate dehydrogenase (GDH) included in the assay mixture.[12,13] Thus, the addition of an Sx_c^- substrate induces an efflux of L-Glu that can be followed fluorometrically in real time. Representative traces (calibrated with a standard curve) for the Sx_c^--mediated exchange of external L-Cys$_2$ with internal L-Glu in SNB19 cells under Na-free conditions is shown in the Figure 3. In

Table 1
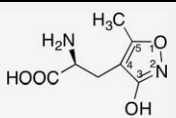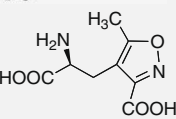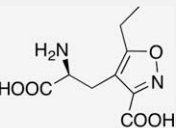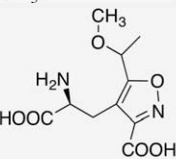Percent of control uptake of L-[³H]-Glu in the presence of ACPA derivatives
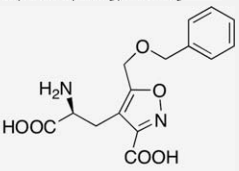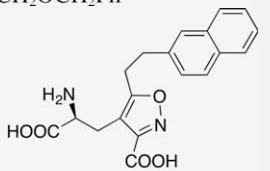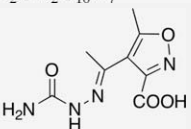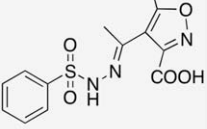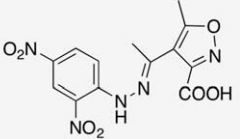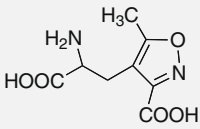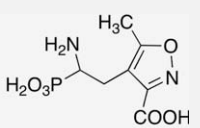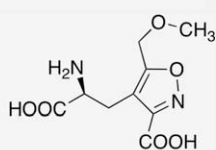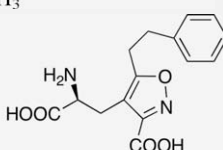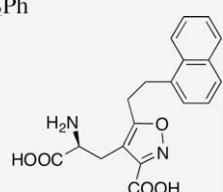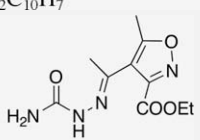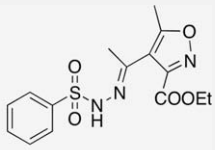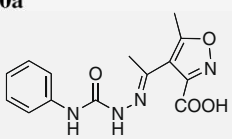
Compound	Sx_c^--mediated ^{3}H-L-Glu uptake
(S)-AMPA **6**	95 ± 2%[a]
(S)-ACPA **7**, R = CH₃	98 ± 12 (n = 3)
(S)-Ethyl-ACPA **7a**, R = CH₂CH₃	92 ± .5 (n = 3)
(R,S)-MeO-Et-(S)-ACPA, **7c** R = (RS)-CH(CH₃)OCH₃	115 ± 12 (n = 3)
BOM-ACPA **7e**, R = CH₂OCH₂Ph	70 ± 6 (n = 4)
S-2-Napthyl-Ethyl-ACPA **7g**, R = **2**-CH₂CH₂C₁₀H₇	37 ± 4 (n = 4)
Semicarbazide free acid, **9b**	91 ± 8 (n = 3)
Benzene Sulfonyl Hydrazone Acid , **10a**	101 ± 15 (n = 3)
2,4-DNP Isoxazole acid, **11d**	73 ± 3 (n = 3)

Table 1 (*continued*)

Compound	Sx_c^--mediated ^{3}H-L-Glu uptake
ACPA (racemic), **7** R = CH₃	101 ± 6 (n = 3)
Amino-Phosphonate-ACPA (racemic) **8**	107 ± 5 (n = 3)
(S)-MOM-ACPA, **7b** R = CH₂OCH₃	98 ± 4 (n = 3)
(S)-Phenyl-ACPA **7d** R = CH₂CH₂Ph	70 ± 5 (n = 3)
S-1-Napthyl-Ethyl-ACPA **7f**, 1-R = CH₂CH₂C₁₀H₇	47 ± 2 (n = 4)
Semicarbazide ester **9a**	103 ± 4 (n = 3)
Benzene Sulfonyl Hydrazone Ester, **10a**	96 ± 5 (n = 3)
Phenyl-Semicarbazide Hydrazone Acid, **9c**	76 ± 5 (n = 3)

SNB-19 cells were assayed for L-[³H]-Glu (100 μM) uptake under Cl-dependent (Na-free) conditions in the presence of ACPA derivatives (250 μM). Values are reported as mean ± SEM ($n \geqslant 3$) of control activity (accumulation in the absence of inhibitors, i.e. 100%). Rates of uptake in these control assays was 573 ± 16 pmol/min/mg protein (mean ± SEM, n = 22).

[a] AMPA was previously assessed for inhibitory activity at 500 μM in LRM55 cells[12] and is included for comparative purposes.

Table 2
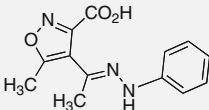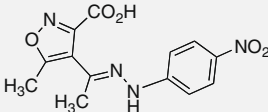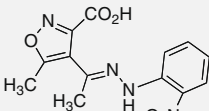Percent of control uptake of L-[³H]-Glu in the presence of isoxazole–hydrazone derivatives
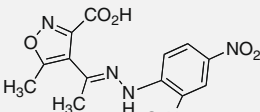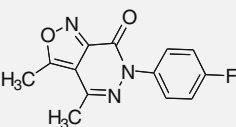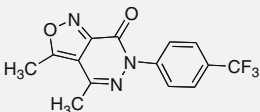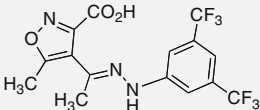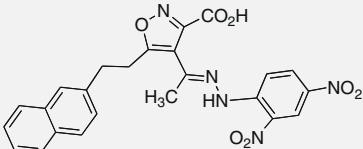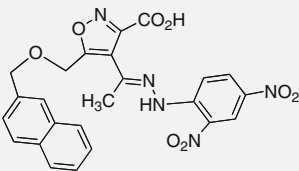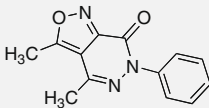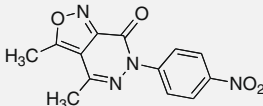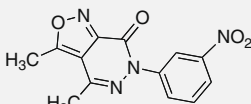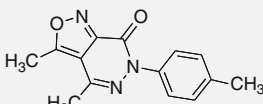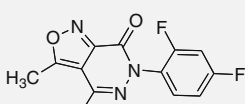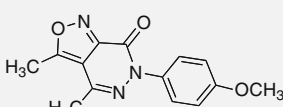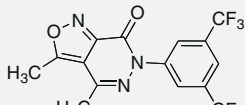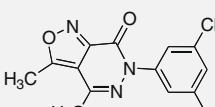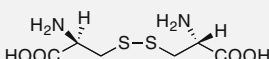
Compound	Sx_c^--mediated ³H-L-Glu uptake
11a, X=Y=Z= H	56 ± 2
11b, X=Y= H, Z= NO₂	22 ± 0.3
11c, X= NO₂, Y=Z= H	97 ± 2
11d, X= Z= NO₂, Y= H	45 ± 1
13f	86 ± 2
13e	99 ± 2
11e	14 ± 4
16a, 2-Naphthyl ethyl	45 ± 2
17, 2-Naphthyl methoxy-Methyl	95 ± 6

Table 2 (continued)

Compound	Sx_c^--mediated ³H-L-Glu uptake
13a, X=Y=Z= H	74 ± 4
13b, X=Y= H, Z= NO₂	85 ± 1
13h	96 ± 2
13c X=Y= H, Z= CH₃	94 ± 3
13g	95 ± 3
13d	92 ± 4
13j	82 ± 6
13i	89 ± 8
L-Cystine	13 ± 1

SNB-19 cells were assayed for L-[³H]-Glu (100 μM) uptake under Cl-dependent (Na-free) conditions in the presence of isoxazole–hydrazone derivatives (500 μM). Values are reported as mean ± SEM (n ⩾ 3) of control activity (accumulation in the absence of inhibitors, i.e. 100%). Rates of uptake in these control assays was 573 ± 16 pmol/min/mg protein (mean ± SEM, n = 22).

contrast to L-Cys₂, the addition of S-2-naphthyl-ethyl-ACPA (**7g**) did not induce an efflux of L-Glu over background levels, indicating that it is not a substrate of the transporter. Consistent with the action of a competitive inhibitor, however, the inclusion of **7g**
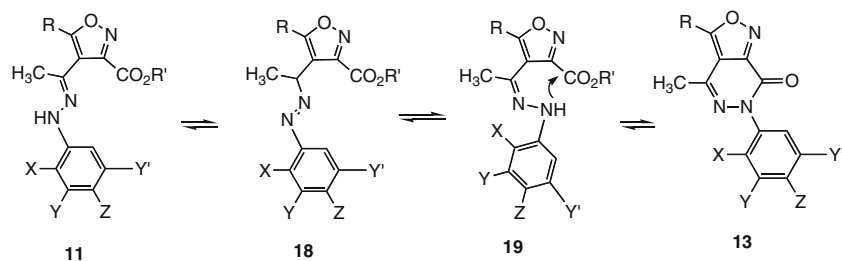
Scheme 2. E- to Z-conversion of **11**, **16**, and **17** likely occurs via tautomerization to a diazene **18**, and the Z-geometry **19** can close rapidly to the isoxazolo[3,4-d] pyridazinone **13**.

Table 3
K_i values for the competitive inhibition of Sx_c^--mediated uptake of L-Glu

Compound		Ki (μM)
7f S-1-Napthyl-ethyl-ACPA		117 ± 15
7g S-2-Napthyl-ethyl-ACPA		52 ± 5
11b		60 ± 2
11e		64 ± 6
11d		147 ± 26
16a		113 ± 7
L-Cystine		59 ± 10

SNB-19 cells were assayed for L-[^{3}H]-glutamate uptake under Cl-dependent (Na-free) conditions in the presence of a range of inhibitor concentrations (10–1000 μM). K_i values were determined in one of to ways: (i) directly from a replot of $K_{m,app}$ values determined by non-linear curve fitting of saturation curves (see Fig. 2) or from IC_{50} values, determined in inhibition curves (see Fig. 1), using the Cheng–Prusoff equation.[37,38] Values are reported as mean ± SEM, $n \geqslant 3$.

Figure 1. IC_{50} determination for selected hydrazone inhibitors. SNB-19 cells were assayed for L-[^{3}H]-glutamate uptake under Cl-dependent (Na-free) conditions in the presence of a range of inhibitor concentrations (10–1000 μM). Data are plotted as mean ± SEM of control activity (accumulation in the absence of inhibitors, i.e., 100%) and were pooled from at least three different assays. IC_{50} values were determined by non-linear curve fitting (KaleidaGraph) and are reported in the inset.
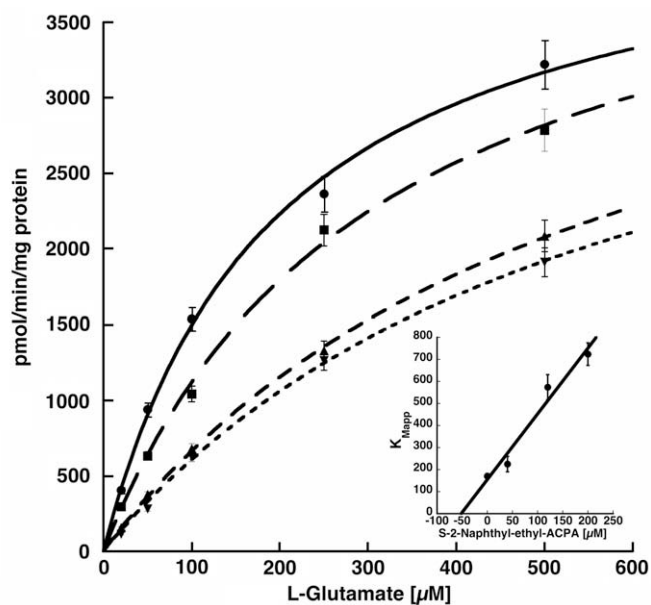
Figure 2. Representative Michaelis–Menten analysis and K_i determination for S-2-naphthyl-ethyl-ACPA. SNB-19 cells were assayed for L-[^{3}H]-glutamate uptake (20, 50, 100, 250, 500 μM) under Cl-dependent (Na-free) conditions in the presence of a range of inhibitor concentrations (20, 40, 200 μM). Data are plotted as pmol/mg/ mg protein and have been corrected for non-specific uptake and leakage. $K_{m,app}$ values were determined by non-linear curve fitting of the saturation curves (KaleidaGraph). K_i values were determined from a replot of $K_{m,app}$ versus [I] as shown in the inset.

did attenuate the ability of L-Cys$_2$ to exchange with intracellular L-Glu. When each of the identified isoxazole inhibitors listed in Table 3 was tested in this manner, none produced an efflux of L-Glu that was significantly different from background. These finding suggest that while the substrate binding site can accommodate the variously modified isoxazoles, the compounds carrying these lipophilic additions cannot be translocated across the membrane.
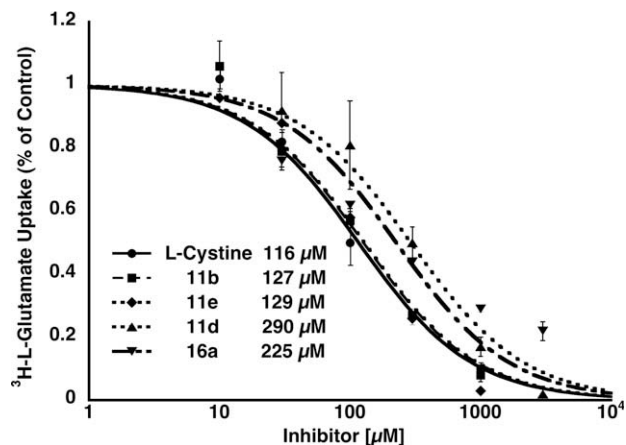
Figure 3. Representative fluorescent traces of Sx_c^--mediated exchange of extracellular substrates for intracellular L-glutamate in SNB-19 cells. Representative fluorometric assays following the substrate-mediated efflux of glutamate from SNB-19 cells under Na+-free conditions as described in Methods. The traces were calibrated using a standard curve in which aliquots of L-glutamate were added to the assay mixture in the absence of the SNB-19 cells. The addition of L-cystine (500 μM) produced a significant efflux of L-glutamate over baseline (absence of any addition), while S-2-naphthyl-ACPA (500 μM) did not. Consistent with a non-substrate inhibitor, S-2-naphthyl-ACPA did, however, attenuate L-cystine-induced efflux when both were added simultaneously.
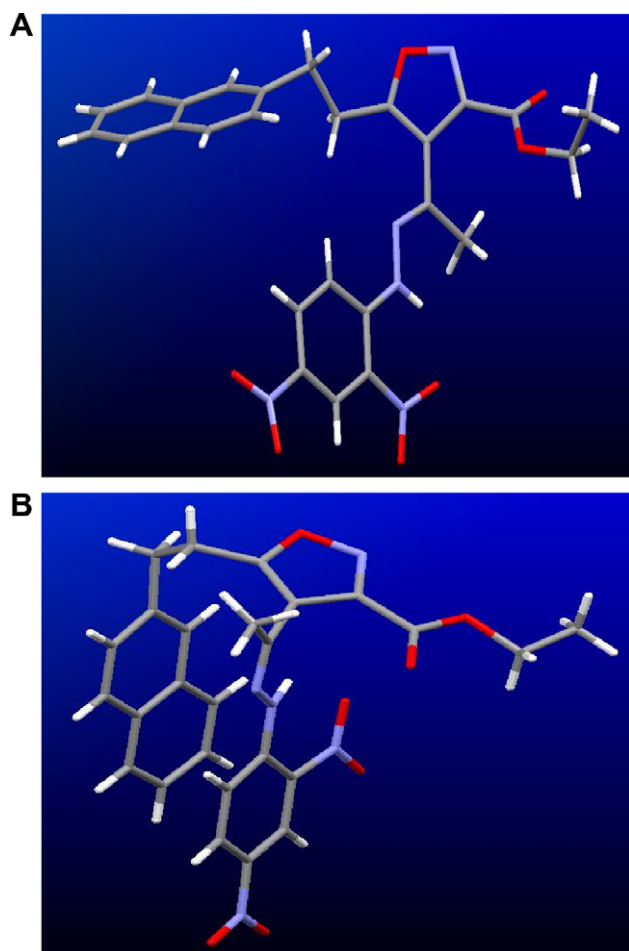
Figure 4. Panel A, X-ray structure of E-**14a**. Panel B. X-ray structure of Z-**14b**.

2.5. Computational modeling of the Sx_c^- binding domain: preliminary pharmacophore model

As a suitable crystal structure is lacking for the development of an Sx_c^- protein homology model, our approach has involved the construction of a ligand-based, superposition, three-dimensional (3D) pharmacophore model. Such models account for structural and functional group similarities in addition to select low energy ligand conformations that have been positioned in 3D space and can be correlated to the SAR data generated from the Sx_c^- transport assays. A similar approach has been successfully employed for delineating potent and selective ligands for the EAATs.[39,40] The ligand training set (Fig. 5, Panel A) included the structurally diverse endogenous substrates L-Glu and L-Cys$_2$ and the potent inhibitors quisqualate (QA) and (S)-4-carboxyphenyl-glycine (4-S-CPG). The latter two provided elements of structural rigidity to the central pharmacophore core region.[12] The model employs both Sx_c^- substrates and non-substrate inhibitors, thereby, allowing it to be consistent with the fundamental hypothesis that an obligate exchange transporter operating with an alternate access mechanism will employ a single substrate binding site that may be defined with discrete overlapping binding domains for the various ligands.

Conformational space searching of the training set ligands afforded global energy minima for the substrates and inhibitors that were then aligned in 3D space to maximize overlap of the α-C, α-COOH, α-NH$_2$, and distal COOH groups or related isosteric moieties. Alignment of the training set L-α-amino acid head groups affords the initial composite superposition pharmacophore model shown in Figure 5, Panel B. A key model aspect is the pseudo chair-like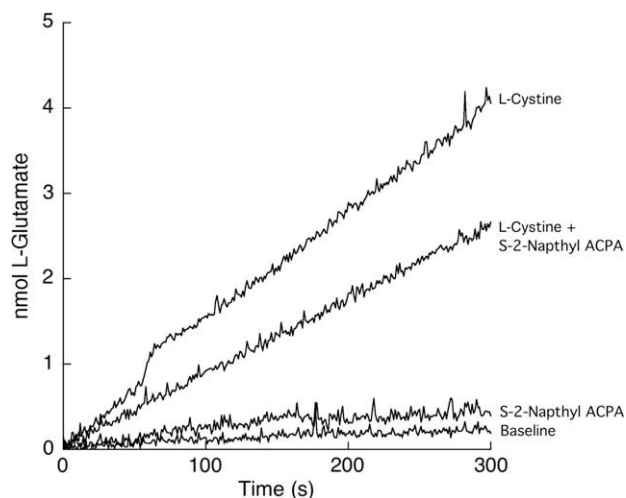 conformations of the substrate L-Cys$_2$ (Panels B–D), which are thought to correlate to the central core ring structures of QA and 4-S-CPG. With the amino acid head groups aligned, the model suggests the likelihood that there may be two ways in which the binding site can accommodate the distal COOH group (or isosteric moieties) as represented in Panels B–D. Although the distal COOH of L-Cys$_2$ could reach either of these positions, based upon rotation about the C6–7 bond (Fig. 5, Panels C and D), we have utilized the L-Cys$_2$ conformation per Panel C in the model, since it is consistent with a conformation in which intramolecular interactions between the 4-position sulfur atom and a proton of the C7 terminal amine group afford an intramolecular hydrogen bonding interaction (depicted in Panel A, ligand **2**) that is supported by NMR spectroscopy.[41,42] The distances between the various COOH binding domains (e.g., Panels C or D as C–C distances between the respective COOH carbon atoms) are distinct from those of L-aspartate and L-α-aminoadipate, further rationalizing the inactivity of L-aspartate as an inhibitor and the activity of L-α-aminoadipate as a substrate.[12] It is also notable that the conformational rigidity of the central rings of 4-S-CPG and QA may provide more optimal Sx_c^- binding as reflected by lower K_i values (e.g., ≈5 μM). The lack of flexibility due to the rings, however, may also account for decreased substrate activity.[12] Thus, 4-S-CPG is essentially a non-substrate inhibitor and QA exchanges with L-Glu at a rate of only 35% that of L-Cys$_2$.

Three compounds of interest were incorporated into the initial pharmacophore model, **7g** and **11e** (both of which exhibited K_i values comparable to L-Cys$_2$), as well as 16a, to identify previously unrecognized regions of the transporter protein that are able to accommodate lipophilic groups and steric bulk. Identifying and optimizing such interactions has been key to the development of high-affinity ligands for the EAATs.[43] The challenge in trying to understand the relative position these lipophilic substituents with respect to the Figure 5 Panels A–D model lies with deciding how to appropriately pair the two COOH groups of these newer compounds with the α- and distal COOH model moieties. Of the three lead inhibitors, only **7g** possesses an L-α-amino acid head group.
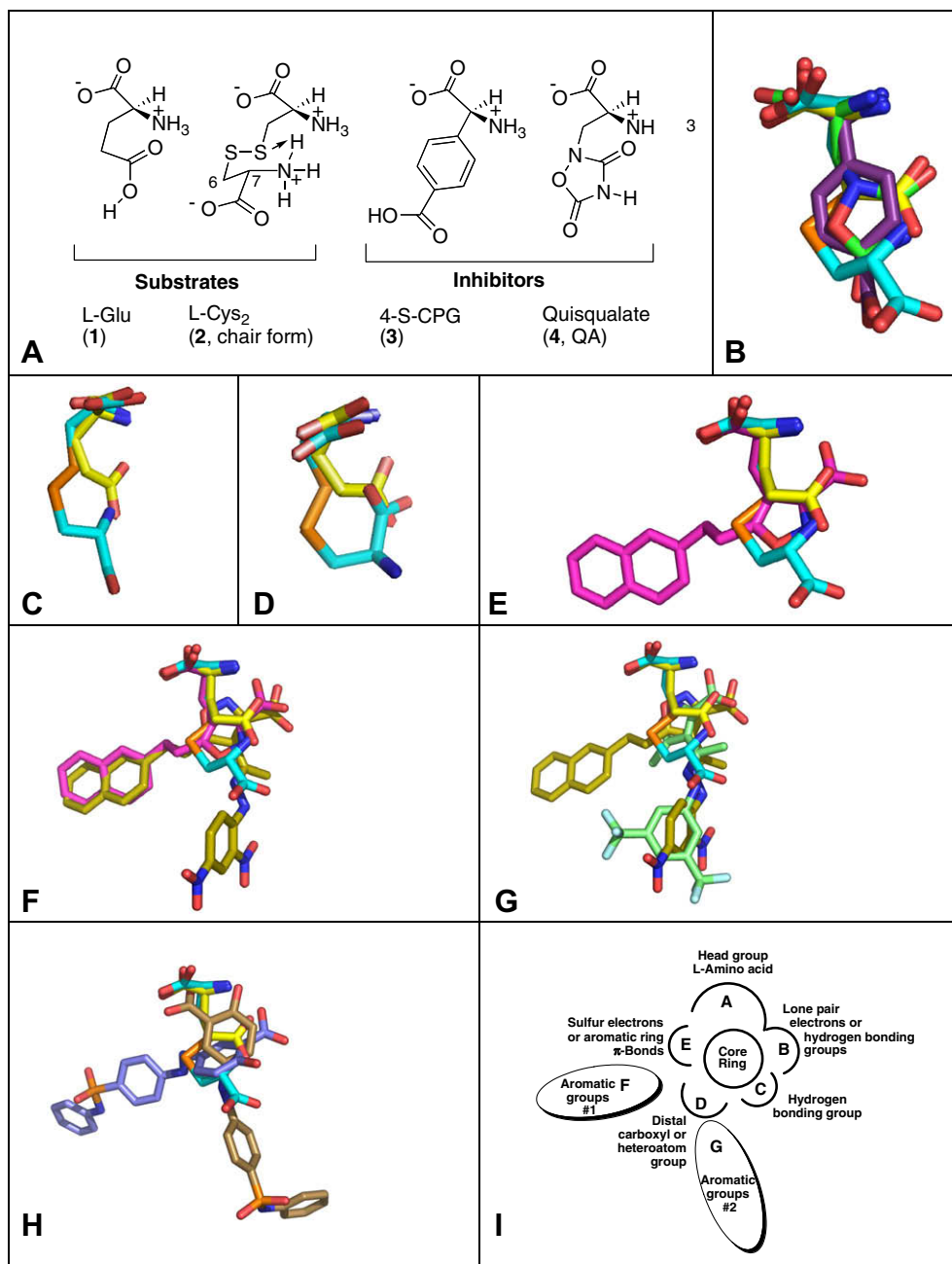
Figure 5. A ligand-based, superposition, three-dimensional (3D) pharmacophore model of the Sx_c^- binding site. Panel A: ligand training set. Panels B–D: L-Glu, **1**, yellow; L-Cys₂, **2**, aqua; 4-S-CPG, **3**, purple; quisqualate, **4**, green. New lead compounds: Panel E, **7g**, violet; Panel F, **7g**, violet and hybrid **16a**, tan; Panel G, hybrid **16a**, tan and **11e**, light green. Panel H: sulfasalazine, **5**, lipophilic group orientations, #1, purple and #2, tan. Panel I, summation pharmacophore cartoon model.

When the α-C, α-COOH and α-NH₂ of **7g** are aligned with the corresponding groups of the initial superposition model, the naphthyl ring moiety occupies the position as shown in Panel E of Figure 5. When the naphthyl moiety position of **7g** is used as a common 3D descriptor for the same naphthyl moiety type of **16a**, then the 3-COOH group extending from the isoxazole ring of **16a** is correlated to the distal COOH group of L-Glu within the model, resulting in a second lipophilic model domain defined by the region occupied by the 2,4-dinitrophenyl moiety, as shown in Figure 5, Panel F. In a similar way, alignment of the 3,5-bis-trifluoromethyl-phenyl group of **11e** with the 2,4-dinitrophenyl group of **16a** aligns the 3-COOH group extending from the isoxazole ring of **16a** to the distal COOH moiety of L-Glu (Fig. 5, Panel G). Although the above lipophilic group alignments are consistent to each other, it is

acknowledged that regions occupied by the respective lipophilic moieties could be reversed resulting in altered alignments of the COOH groups and related isosteric moieties.

Similar alignment ambiguity arises when the more recently identified inhibitor sulfasalazine **5** (5-[4-(2-pyridylsulfamoyl)phenylazo]salicylic acid) is incorporated into the model. This compound has attracted considerable attention because it provides a potential therapeutic link between Sx_c^- inhibition and the treatment of CNS glial tumors.[5,44] Thus, the pyridylsulfamoylphenyl portion of sulfasalazine can be correlated to either of the lipophilic regions defined by **7g**, **11e**, or **16a** depending upon whether the COOH group of the salicylic moiety of **5** is aligned with the α- or distal COOH group of L-Glu (Fig. 5, Panel H). Since either model alignments are possible with sulfasalazine, then it is thought that the lipophilic domains

extending beyond the core Sx_c^- substrate binding area imparts enhanced Sx_c^- binding. Thus, while the parent analogues (e.g., ACPA (**7**), S-ethyl-ACPA (**7a**)) exhibit little or no activity, the inclusion of lipophilic groups with sufficient π-electron character and steric bulk at the C5 of the isoxazole ring or via a hydrazone linkage to the free amino group of ACPA, or both, markedly enhances the ability of these ligands to bind to the Sx_c^- site.

The ligand alignment computational modeling and SAR insights have allowed us to generate an initial perspective of an Sx_c^- pharmacophore model. A composite cartoon representation of the model is shown in Figure 5, Panel I. The model central core ring area is consistent with the notion that an alternate access transporter can be defined with discrete overlapping binding domains for the various ligands. The model regions that surround the central core ring area include: (a) the L-amino acid head group; (b) an electron lone pair region or a hydrogen bonding group, equivalent to the distal COOH group of L-Glu or a heteroatom of the isoxazole ring of the analogues; (c) a hydrogen bonding group, equivalent to the distal L-amino acid moiety of L-Cys$_2$ or a second heteroatom of an isoxazole ring within an analogue, (d) a distal carboxyl or heteroatom area, equivalent to the distal COOH group of L-Cys$_2$ or 4-S-CPG; (e) lone pair electron or π-electron density, associated with the sulfur atoms of L-Cys$_2$ or the aromatic ring of 4-S-CPG; (f) an aromatic ring group region #1 which is represented by analogue **7g**; and (g) an aromatic ring group region #2 which found in analogue **16a**. Importantly, not all of the pharmacophore regions A–G need to be represented in each ligand to produce significant Sx_c^- binding. Additionally, higher affinity Sx_c^- ligands may possess different select combinations of the model A–G structural facets.

As previously mentioned, the increased inhibitory activity of EAAT ligands possessing lipophilic groups has been similarly used to infer the presence lipophilic domains adjacent to transporter substrate binding sites. Interestingly, for both the EAAT and Sx_c^- transporters, the interactions between these lipophilic domains and the ligands is also associated with a decreased ability of the appended analogues to act as alternative substrates. Taken together, our initial SAR-based pharmacophore model supports a single site hypothesis for Sx_c^- in which functional groups on identified substrates and inhibitors most likely interact with different subsets of available binding domain residues or the same residues in the binding site altered with different relative conformations. This is perhaps best illustrated by inhibitors such as **11e** and sulfasalazine, which may be binding to Sx_c^- in a manner that does involve the L-α-amino acid head group area, and that also is defined by the endogenous L-Glu and L-Cys$_2$ substrates for the transporter.

3. Conclusions

In summary, analogues of AMPA have been prepared that bind the Sx_c^- transporter, with the most efficacious analogues amino acid **7g** and bioisostere **11e** having comparable activity to the endogenous substrate cystine. Both classes of compounds appear to exhibit competitive binding. The isoxazolo[3,4-d] pyridazinones **13**, in contrast exhibit only very weak binding at the Sx_c^- antiporter, although examination of their binding at other stages of the glutamate–glutamine cycle could be worthwhile. Experiments to address these and related model-derived questions are planned to significantly advance the discovery paradigm. Future targets of second generation refined Sx_c^- inhibitor analogues will further elucidate which combinations of regions of the pharmacophore model provide the greatest Sx_c^- binding potency. Of particular interest will be the further characterization of the lipophilic ligand domains discovered in the present study.

4. Experimental section

Commercial reagents are routinely examined for purity by NMR and TLC, and recrystallized or distilled as appropriate. All reactions were monitored by TLC. NMR was performed on a Varian Unity Plus spectrometer at (400 MHz for ^{1}H, 101 MHz for ^{13}C) in deuterochloroform unless otherwise noted. Chemical shifts (δ) are reported using CHCl$_3$ (7.26 ppm for ^{1}H), CDCl$_3$ (77 ppm for ^{13}C) as references. High resolution mass spectra (HRMS) were obtained using a Micromass electrospray ionization (ESI)/time-of-flight mass spectrometry (LC–TOF). Mass spectrometer samples were introduced using a Waters model 2690 separations module HPLC fitted with a C-18 reversed phase column (2.1 mm id, 5 cm). Elemental analyses for C, H, and N were performed by Midwest Microlab, Indianapolis, IN. Melting points were uncorrected.

4.1. Chemistry: amino acid analogues of AMPA

Amino acids, racemic ACPA ((±)-**7**),[45] (±)-**8** (S)-ACPA, ((−)-**7**), **7d**, **7g**, **7f**,[19] **7a** and (S,S)-**7c**[18] were prepared using methods previously described by our laboratories, and full experimental details have been published. (S)-MOM-ACPA (**7b**) and BOM-ACPA (**7e**)[46] were prepared from **12** via the known 5-hydroxyl-methyl acetal[18] using the amino acid synthesis sequence previously described.[19]

4.1.1. 4-[(2S)-2-Amino-2-carboxyethyl]-5-[methoxymethyl] isoxazole-3-carboxylic acid (7b, (S)-MOM-ACPA)

Overall yield 12% for four steps, **7b** was obtained as 60 mg of a yellowish solid, mp = 166–168 °C (dec.). ^{1}H NMR (D$_2$O) δ 3.25 (dd, 1H), 3.38 (dd, 1H), 3.41 (s, 3H), 4.29 (t, 1H, J = 6.8 Hz), 4.65 (s, 2H).^{13}C NMR δ 23.8, 53.6, 59.4, 63.8, 113.0, 157.3, 164.0, 169.8, 171.9 FAB$^+$ (m-glycerol) m/z 245 [M+1]$^+$ (38.8% rel. intensity-glycerol matrix gave base peak at m/z 74.79). Anal. Calcd C$_9$H$_{13}$N$_2$O$_6$ [M+1]$^+$ mass: 245.077361. Accurate mass: FAB$^+$ 245.0769. Optical rotation: $[\alpha]_D^{20}$ −5.3 (c 0.15, H$_2$O). Anal. Calcd for C$_9$H$_{13}$N$_2$O$_6$Cl: C, 38.51; H, 4.66; N, 9.98. Found: C, 38.51; H, 4.52; N, 9.73.

4.1.2. 4-[(2R,S)-2-Amino-2-carboxyethyl]-5-[benzyloxymethyl] isoxazole-3-carboxylic acid (7e, BOM-ACPA)

Overall yield 7% for four steps, **7e** was obtained as 40 mg of a yellowish solid, mp = 166–168 °C (dec.). ^{1}H NMR (DMSO-d$_6$) δ 2.97 (dd, 1H), 3.16 (dd, 1H), 3.92 (t, 1H, J = 5.75 Hz), 4.55 (s, 2H), 4.65 (q, 2H, J = 13.05 Hz), 7.37 (m, 5H).^{13}C NMR (126 MHz) δ 23.5, 30.5, 33.02, 52.0, 58.5, 60.8, 63.4, 71.8, 110.8, 127.5, 128.1, 161.3, 170.1 FAB$^+$ (m-glycerol/DMSP) m/z 321 [M+1]$^+$, 277, 219, 91.6 Anal. Calcd for C$_{15}$H$_{16}$N$_2$O$_6$ (1.5 H$_2$O): C, 51.87; H, 5.51; N, 8.06. Found: C, 51.48; H, 4.81; N, 8.80. HRMS calcd C$_{15}$H$_{17}$N$_2$O$_6$ [M+1]$^+$: 321.1087, found: FAB$^+$ 321.1073.

4.2. Chemistry bioisosteres of AMPA

Common intermediate **12** was prepared as described by dal Piaz.[21] Isoxazolo[3,4-d]pyridazinone **13a** is known, also from that group's extensive work in the area.[22–32] Compounds **13b–d** and **13f–g**, and **13j** are reported in Chemical Abstracts, and are commercially available from Ryan Scientific, Inc., but are not referenced to Patent or Publication literature, therefore, the CAS registry number and full characterization data is provided for each in the Supplementary data. Open hydrazones **11a–e** were prepared in analogous fashion as previously described by our laboratories.[20]

4.3. 5-Methyl-4-[1-(phenyl-hydrazono)-ethyl]-isoxazole-3-carboxylic acid (11a)

Light brown solid; yield = 60%; mp = 138 °C; ^{1}H NMR (CD$_3$OD) δ 2.18 (s, 3H), 2.58 (s, 3H), 6.78 (t, J = 8 Hz, 1H), 7.12 (d, J = 8.0 Hz,

2H), 7.19 (t, J = 8 Hz, 2H); ^{13}C NMR (CD$_3$OD) δ 12.3, 16.6, 114.2 (3C), 120.8, 130.1 (3C), 134.9, 147.3, 163.5, 170.0; MS (ES+) 260 (M+1), HRMS calcd for C$_{13}$H$_{14}$N$_3$O$_3$ [M+H]$^+$ 260.1035, found 260.1021.

4.4. 5-Methyl-4-{1-[(4-nitro-phenyl)-hydrazono]-ethyl}-isoxazole-3-carboxylic acid (11b)

Yellow solid; yield = 72%; mp = 240 °C; ^{1}H NMR (acetone-d_6) δ 2.36 (s, 3H), 2.61 (s, 3H), 7.93 (d, J = 8.0 Hz, 2H), 8.44 (d, J = 8.0 Hz, 2H); ^{13}C NMR (acetone-d_6) δ 11.7, 16.1, 111.8, 112.2 (2C), 125.9 (2C), 138.8, 140.1, 151.2, 155.0, 161.4, 169.1; MS (ES+) 305 (M+1), HRMS calcd for C$_{13}$H$_{13}$N$_4$O$_5$ [M+H]$^+$ 305.0886, found 305.0901.

4.5. 5-Methyl-4-{1-[(2-nitro-phenyl)-hydrazono]-ethyl}-isoxazole-3-carboxylic acid (11c)

Orange solid; yield = 97%; mp = 168–169 °C; ^{1}H NMR (acetone-d_6) δ 2.36 (s, 3H), 2.65 (s, 3H), 6.96 (m, 1H), 7.64 (m, 1H), 7.89 (d, J = 8.0 Hz, 1H), 8.18 (d, J = 8.0 Hz, 1H), 10.86 (br s, 1H); ^{13}C NMR (acetone-d_6) δ 11.6, 16.0, 116.0, 118.8 (2C), 125.9 (2C), 136.6 (2C), 141.2, 154.9, 161.3, 169.6; MS (ES+) 305 (M+1), HRMS calcd for C$_{13}$H$_{13}$N$_4$O$_5$ [M+H]$^+$ 305.0886, found 305.0903.

4.6. 4-{1-[(2,4-Dinitro-phenyl)-hydrazono]-ethyl}-5-methyl-isoxazole-3-carboxylic acid (11d)

Red solid; yield = 66%; mp = 189–191 °C; ^{1}H NMR (CD$_3$OD) δ 2.39 (s, 3H), 2.64 (s, 3H), 7.96 (d, J = 8.0 Hz, 1H), 8.38 (d, J = 8.0 Hz, 1H), 9.07 (s, 1H); ^{13}C NMR (CD$_3$OD) δ 12.4, 17.1, 70.6, 117.2, 117.6 (2C), 124.1 (2C), 131.2 (2C), 146.2, 146.9, 171.5; MS (ES+) 350 (M+1), HRMS calcd for C$_{13}$H$_{12}$N$_5$O$_7$ [M+H]$^+$ 350.0737, found 350.0767. Anal. Calcd for C$_{13}$H$_{12}$N$_5$O$_7$ (1.5 H$_2$O): C, 41.49; H, 3.75; N, 18.61. Found: C, 41.46; H, 3.47; N, 18.01.

4.7. 4-{1-[(3,5-Bis-trifluoromethyl-phenyl)-hydrazono]-ethyl}-5-methyl-isoxazole-3-carboxylic acid (11e)

Off white solid; yield = 95%; mp = 137–139 °C; ^{1}H NMR (acetone-d_6) δ 2.28 (s, 3H), 2.59 (s, 3H), 7.33 (s, 1H), 7.71 (s, 2H), 9.41 (br s, 1H); ^{13}C NMR (acetone-d_6) δ 11.5, 16.4, 111.5, 112.6 (2C), 116.6, 131.9 (2C), 138.7 (2C), 147.5, 156.3, 162.3, 168.5, 185.5; MS (ES+) 396 (M+1), HRMS calcd for C$_{15}$H$_{12}$N$_3$O$_3$F$_6$ [M+H]$^+$ 396.0783, found 396.0801.

4.8. 3,4-Dimethyl-6-(4-(trifluoromethyl)phenyl)isoxazolo[3,4-d]pyridazin-7(6H)-one (13e)

Brown crystalline solid; yield = 28% mp = 161–163 °C; ^{1}H NMR δ 2.56 (s, 3H), 2.90 (s, 3H), 7.72 (d, J = 8 Hz, 2H), 7.78 (d, J = 8 Hz, 2H); ^{13}C NMR δ 13.5, 19.8, 37.0, 112.6, 126.2, 129.7, 129.9, 141.1, 143.8, 152.5, 153.2, 170.6; MS (ES+) 310 (M+1), HRMS calcd for C$_{14}$H$_{11}$N$_3$O$_2$F$_3$ [M+H]$^+$ 310.0803, found 310.0771.

4.9. 3,4-Dimethyl-6-(3-nitrophenyl)isoxazolo[3,4-d]pyridazin-7(6H)-one (13h)

White solid; yield = 96% mp = 187–188 °C; ^{1}H NMR δ 2.59 (s, 3H), 2.91 (s, 3H), 7.63 (m, 1H), 8.07 (m, 1H), 8.21 (m, 1H), 8.54 (s, 1H); ^{13}C NMR δ 13.5, 19.8, 112.6, 121.1, 122.5, 129.6, 131.7, 141.6, 141.8, 152.4, 153.2, 170.8; MS (ES+) 287 (M+1), HRMS calcd for C$_{13}$H$_{11}$N$_4$O$_4$ [M+H]$^+$ 287.0780, found 287.0785.

4.10. 3,4-Dimethyl-6-(3,5-dichlorophenyl)isoxazolo[3,4-d]pyridazin-7(6H)-one (13i)

White solid; yield = 93% mp = 230–232 °C; ^{1}H NMR (400 MHz, CDCl$_3$) δ 2.56 (s, 3H), 2.89 (s, 3H), 7.34 (s, 1H), 7.59 (s, 2H); ^{13}C NMR (100 MHz, CDCl$_3$) δ 13.5, 19.8, 112.5, 124.5 (2C), 128.1 (2C), 135.1, 141.2, 142.4, 152.4, 153.0, 170.7; MS (ES+) 310 (M+), 312 (M+2); HRMS calcd for C$_{13}$H$_{10}$N$_3$O$_2$Cl$_2$ [M+H] 310.0150, found 310.0190.

4.11. 4-{1-[(2,4-Dinitro-phenyl)-hydrazono]-ethyl}-5-(2-naphthalen-2yl-ethyl)-isoxazole-3-carboxylic acid ethyl ester (14)

To a solution of ketone[19] (0.56 g, 1.66 mmol) in THF (10 ml), 2,4-DNP reagent (10.9 ml, 1.66 mmol) was added drop wise at 0 °C. The mixture was stirred at room temperature for 6 h. Precipitate formed was filtered and purified by column chromatography (30% ether in hexanes). The major product was obtained as orange colored solid (14a), yield = 81%, mp = 160 °C; ^{1}H NMR δ 1.43 (t, J = 7.1 Hz, 3H), 1.93 (s, 3H), 3.26 (t, J = 6.8 Hz, 2H), 3.40 (t, J = 6.2 Hz, 2H), 4.44 (q, J = 7.1 Hz, 2H), 7.17 (dd, J = 8.4 & 1.7 Hz, 1H), 7.44 (m, 2H), 7.52 (m, 1H), 7.65 (m, 2H), 7.72 (d, J = 8.4 Hz, 1H), 7.76 (m, 1H), 8.14 (dd, J = 9.5 and 2.6 Hz, 1H), 9.14 (d, J = 2.5 Hz, 1H), 10.98 (br s, 1H, NH). ^{13}C NMR δ 14.1, 17.2, 27.9, 34.0, 62.6, 116.2, 116.7, 123.3, 125.9, 126.4, 126.6, 126.8, 127.2, 127.6, 128.3, 129.9, 130.1, 132.2, 133.4, 136.8, 138.6, 144.5, 144.9, 153.9, 159.9, 172.2; MS (FAB): m/z 518(33), 517 (100), 501 (12), 248 (11), 154 (34), 141 (61), 136 (23).

Anal. Calcd for C$_{26}$H$_{23}$N$_5$O$_7$: C, 60.35; H, 4.48; N, 13.53. Found: C, 60.51; H, 4.62; N, 13.41. Minor product (14b), yellow solid, ^{1}H NMR δ 1.30 (t, J = 8.0 Hz, 3H), 2.08 (s, 3H), 3.21 (m, 4H), 4.32 (q, J = 8.0 Hz, 2H), 7.16 (dd, J = 8.0 and 4.0 Hz, 1H), 7.30 (m, 2H), 7.44 (m, 1H), 7.58 (m, 3H), 7.76 (d, J = 8.0 Hz, 1H), 8.20 (dd, J = 8.0 & 4.0 Hz, 1H), 8.84 (d, J = 4.0 Hz, 1H), 10.37 (br s, 1H, NH).

4.12. 4-{1-[(2,4-Dinitro-phenyl)-hydrazono]-ethyl}-5-(2-naphthalen-2-yl-ethyl)-isoxazole-3-carboxylic acid (16a)

To a solution of 14a (0.65 g) in THF, 2 ml of 3 M NaOH was added drop wise at 0 °C. After 0.5 h stirring the disappearance of ester was observed. The reaction mixture was acidified with 1 M HCl to pH 2 and extracted with EtOAc. The organic extracts were then washed with saturated NaHCO$_3$ followed by brine and finally dried over sodium sulfate. The organic layer was filtered and evaporated. The residue obtained was purified by column chromatography with 5% MeOH in CHCl$_3$ as eluent. The pure product was obtained as yellow solid, yield = 67%, mp = 169–171 °C; ^{1}H NMR (acetone-d_6): δ 2.10 (s, 3H), 3.27 (t, J = 8.0 Hz, 2H), 3.50 (t, J = 8.0 Hz, 2H), 7.34 (dd, J = 8.0 and 4.0 Hz, 1H), 7.41 (m, 2H), 7.66 (m, 1H), 7.71 (m, 1H), 7.79 (m, 2H), 7.88 (d, J = 8.0 Hz, 1H), 8.29 (dd, J = 8.0 and 4.0 Hz, 1H), 9.00 (m, 1H), 10.97 (br s, 1H, NH). ^{13}C NMR (acetone-d_6) δ 16.7, 30.4, 42.0, 94.6, 115.6 (2C), 123.0 (2C), 125.5 (2C), 126.2, 126.7 (2C), 127.5, 127.6, 127.8, 128.2 (2C), 130.5 (2C), 133.9, 134.0, 139.0, 172.7; MS (FAB): m/z 492 (9.0), 491 (33), 490 (100), 489 (32), 460 (27), 446 (51), 445 (25). Anal. Calcd for (C$_{24}$H$_{19}$N$_5$O$_7$)$_2$.H$_2$O: C, 57.83; H, 4.04; N, 14.05. Found: C, 57.74; H, 3.58; N, 13.80.

4.13. 4-{1-[(2,4-Dinitro-phenyl)-hydrazono]-ethyl}-5-(naphthalen-2-ylmethoxymethyl)-isoxazole-3-carboxylic acid (17)

Yield: 60% The major isomer ^{1}H NMR (DMSO) δ 2.34 (s, 3H), 4.74 (s, 2H), 4.89 (s, 2H), 7.65 (d, 1H, J = 9.5 Hz), 7.80 (m, 4H), 7.91 (m, 3H), 8.15 (dd, 1H, J = 2.4, 9.5 Hz), 8.79 (d, 1H, J = 2.6 Hz), 10.87 (br s, 1H, NH). ^{13}C NMR (500 MHz) δ 15.3, 72.3, 73.4, 102.0, 120.9, 125.6, 125.7, 125.8, 125.9, 127.3, 127.5, 127.6,

127.7, 128.2, 129.6, 132.3, 132.6, 134.7, 135.6, 144.6, 146.2, 149.8, 152.7, 190.8. Accurate mass Calcd for $C_{24}H_{20}N_5O_8$ $[M+1]^+$: 506.131187. Found: FAB$^+$ 506.131188.

The minor isomer ^{1}H NMR (DMSO) δ 2.29 (s, 3H), 4.51 (s, 2H), 4.78 (s, 2H), 7.25 (d, 1H, J = 9.5 Hz), 7.42 (m, 4H), 7.54 (m, 3H), 8.40 (dd, 1H, J = 2.4, 9.5 Hz), 8.89 (d, 1H, J = 2.6 Hz), 10.55 (br s, 1H, NH). FAB$^+$ m/z 506 $[M+1]^+$, 490, 349, 306, 288, 272.

4.14. Cell culture

SNB-19 glioma cells, purchased from American Type Culture Collection (Manassas, VA), were grown in Ham's F-10 medium (pH 7.4) containing 1 mM pyruvate and 16 mM NaHCO$_3$ and supplemented with 10% fetal calf serum. The cells were cultured in 150 cm^2 flasks (Corning) and maintained at 37 °C in a humidified atmosphere of 5% CO$_2$. For L-glutamate uptake experiments, cells were seeded in 12 well culture plates (Costar) at a density of 5×10^4 cells/well and for fluorometric assays cells were seeded on 9.5 × 22 mm coverslips at a density of 1×10^5 cells/coverslip and maintained for 5–8 days until 80–90% confluent. Cells formed a confluent monolayer with an estimated density of $1–2.5 \times 10^6$ cells and a protein concentration of 100–350 mg/well or coverslip as determined by the bicinchoninic acid (BCA) method (Pierce). Cells were given fresh medium 2 h prior to an assay.

4.15. Glutamate uptake assay

Uptake of L-glutamate into cultured cells was quantified using a modification of the procedure of Martin and Shane as previously described.[12,13,47] Individual wells, after removal of culture media, were rinsed three times and pre-incubated in 1 ml Na$^+$-free HEPES buffered (pH 7.4) Hank's balanced salt solution (HBHS) at 30 °C for 5 min. The Na$^+$-free buffer contained: 137.5 mM choline Cl, 5.36 mM KCl, 0.77 mM KH$_2$PO$_4$, 0.71 mM MgSO$_4$.7H$_2$O, 1.1 mM CaCl$_2$, 10 mM D-glucose, and 10 mM HEPES. Uptake was initiated by aspiration of the preincubation buffer and the addition of a 500 μl aliquot of Na$^+$-free transport buffer containing L-[^{3}H]-glutamate (4–16 mCi/ml) mixed with L-glutamate (10–500 μM, final concentration). In those assays that evaluated inhibitor activity, the 500 μl aliquot of transport buffer contained both the L-[^{3}H]-glutamate and potential inhibitors to ensure simultaneous addition. Following a 5 min incubation at 30 °C, the assays were terminated by three sequential 1 ml washes with ice cold buffer and then the cells were dissolved in 1 ml of 0.4 M NaOH for 24 h. An aliquot (200 μl) was then transferred into a 5 ml glass scintillation vial and neutralized with the addition of 5 μl glacial acetic acid followed by 3.5 ml Liquiscint@ scintillation fluid (National Diagnostics) to each sample. Incorporation of radioactivity was quantified by liquid scintillation counting (LSC, Beckman LS 6500). Values are reported as mean ± S.E.M and are corrected for non-specific uptake (e.g., leakage and binding) by subtracting the amount of L-[^{3}H]-glutamate accumulation at 4 °C. Inhibitory and Lineweaver–Burk plots and associated kinetic parameters for transport inhibitors were estimated using a non-linear curve fitting analysis (KaleidaGraph 3.6.5). K_i values were estimated on the basis of a replot of $K_{m,app}$ values or using IC$_{50}$ values and the Cheng–Prusoff equation.[37]

4.16. Fluorometric assay

Fluorometric determination of L-glutamate efflux was quantified using a modification of the procedures described by Nicholls et al.[48] and Vesce et al.[49] NADPH fluorescence was quantified using a Hitachi F-2000 fluorescence spectrophotometer fitted with a thermostatted cuvette holder and a 1 cm^2 electronically driven

magnetic stirrer platform. Confluent monolayers of SNB-19 glioma cells grown on coverslips were paired, placed back to back and rinsed in Na$^+$-free HBHS buffer for 10 min. The coverslips were transferred and incubated in a stirred quartz cuvette containing 2 ml HBHS at 30 °C. Assays were initiated with the addition of NADP$^+$ (1 mM) at 0 s followed by GDH (33 U) at 60 s. Subsequent additions of L-cystine or other potential substrates (50–500 μM) were made as detailed in the figure legends. Each experiment was terminated with the addition of Triton X-100 (0.5%) to determine the total amount of L-Glu in the cells. The amount of L-Glu efflux was determined via a standard curve generated in an identical experiment but omitting the cells. Following the enzyme, seven sequential additions of 4 nmol L-Glu were made yielding a non-linear curve. Rates of L-Glu efflux are reported as mean ± S.E.M and are corrected for non-specific efflux (e.g., leakage) by subtracting the amount of L-Glu efflux in the absence of L-cystine.

4.17. Computational modeling

Computational modeling followed methods we have employed previously for the production of a gas phase, steric strain, 3D superposition, ligand-based pharmacophore model.[39,40] Conformational searching and alignment studies were carried out at the University of Montana, Molecular Computational Core Facility. In essence, training set ligands, including substrates L-Glu and L-Cys$_2$ and inhibitors quisqualate (QA) and (S)-4-carboxyphenyl-glycine (4-S-CPG) were built with SYBYL 7.0 software suite (Tripos, Inc.; St. Louis, MO) and subjected to energy minimization (10,000 iterations) by Powell minimization standard method. Initial Optimization and Termination parameters were set to None and Energy Change options, respectively. Default parameters and values within the minimization dialogue (minimize details) were used. Respective ligand conformers were stored as MOL2 files within a molecular spreadsheet and sorted based on energy profile. The low energy conformation was identified per ligand. Similar conformational searches were performed for **7g**, **11e**, **16a** and other analogues. Each low energy analogue per ligand was imported with SYBYL and positioned in 3D space utilizing the following common atoms (centroids) for alignment, (a) amino acid head group: α-carbon, carbon of the COOH group and the amino moiety (α-NH$_2$), and (b) the distal COOH group carbon. When necessary, isosteric groups were directly correlated to the above alignment moieties. The various composite alignments were inspected visually in 3D and checked for desired atom superposition. Composite MOL2 files were exported to MacPyMol software (Version 0.99; DeLano Scientific, LLC; South San Francisco, CA) to provide the Figure 5 molecular renderings.

Supplementary data

Supplementary data associated with this article can be found, in the online version, at doi:10.1016/j.bmc.2009.11.001.

References and notes

1. Balazs, R.; Bridges, R. J.; Cotman, C. W. *Excitatory Amino Acid Transmission in Health and Disease*; Oxford University Press: New York, 2006.
2. Kranich, O.; Dringen, R.; Sandberg, M.; Hamprecht, B. *Glia* **1998**, *22*, 11.
3. Baker, D. A.; McFarland, K.; Lake, R. W.; Shen, H.; Tang, X. C.; Toda, S.; Kalivas, P. W. *Nat. Neurosci.* **2003**, *6*, 743.
4. Knackstedt, L. A.; Larowe, S.; Mardikian, P.; Upadhyaya, H.; Hedden, S.; Markou, A.; Kalivas, P. *Biol. Psychiat.* **2008**. Epub.
5. Chung, W. J.; Lyons, S. A.; Nelson, G. M.; Hamza, H.; Gladson, C. L.; Gillespie, G. Y.; Sontheimer, H. *J. Neurosci.* **2005**, *25*, 7101.
6. Shih, A.; Erb, H.; Sun, X.; Toda, S.; Kalivas, P.; Murphy, T. *J. Neurosci.* **2006**, *41*, 10514.
7. Espey, M. G.; Kustova, Y.; Sei, Y.; Basile, A. S. *J. Neurochem.* **1998**, *71*, 2079.
8. Hosoya, K.; Tomi, M.; Ohtsuki, S.; Takanaga, H.; Saeki, S.; Kanai, Y.; Endou, H.; Naito, M.; Tsuruo, T.; Terasaki, T. *J. Pharmacol. Exp.Therapeut.* **2002**, *302*, 225.
9. Baker, D. A.; Xi, Z. X.; Hui, S.; Swanson, C. J.; Kalivas, P. W. *J. Neurosci.* **2002**, *22*, 9134.
10. Augustin, H.; Grosjean, Y.; Chen, K.; Sheng, Q.; Featherstone, D. *J. Neurosci.* **2007**, *27*, 111.
11. Bannai, S. *J. Biol. Chem.* **1986**, *261*, 2256.
12. Patel, S. A.; Warren, B. A.; Rhoderick, J. F.; Bridges, R. J. *Neuropharmacology* **2004**, *46*, 273.
13. Warren, B. A.; Patel, S. A.; Nunn, P. B.; Bridges, R. J. *Toxicol. Appl. Pharmacol.* **2004**, *200*, 83.
14. Cho, Y.; Bannai, S. *J. Neurochem.* **1990**, *55*, 2091.
15. Ye, Z.; Rothstein, J. D.; Sontheimer, H. *J. Neurosci.* **1999**, *19*, 10767.
16. Madsen, U.; Slok, F. A.; Stensbol, T. B.; Brauner-Osborne, H.; Lutshoft, H. H.; Poulsen, M. V.; Eriksen, L.; Krogsgaard-Larsen, P. *Eur. J. Med. Chem.* **2000**, *35*, 447.
17. Brauner-Osborne, H.; Egebjerg, J.; Nielsen, E. O.; Madsen, U.; Krogsgaard-Larsen, P. *J. Med. Chem.* **2000**, *43*, 2609.
18. Nelson, J. K.; Twamley, B.; Villalobos, T. J.; Natale, N. *Tetrahedron Lett.* **2008**, *49*, 5957.
19. Burkhart, D. J.; McKenzie, A. R.; Nelson, J. K.; Myers, K. I.; Zhao, X.; Magnusson, K. R.; Natale, N. R. *Org. Lett.* **2004**, *6*, 1285.
20. Burkhart, D. J.; Vij, A.; Natale, N. R. *J. Chem. Crystallogr.* **1999**, *29*, 749.
21. Renzi, G.; Dal Piaz, V. *Gazz. Chim. Ital.* **1965**, *95*, 1478.
22. Costantino, L.; Rastelli, G.; Gamberini, M. C.; Giovannoni, M. P.; Dal Piaz, V.; Vianello, P.; Barlocco, D. *J. Med. Chem.* **1999**, *42*, 1894.
23. Dal Piaz, V.; Castellana, M. C.; Vergelli, C.; Giovannoni, M. P.; Gavalda, A.; Segarra, V.; Beleta, J.; Ryder, H.; Palacios, J. M. *J. Enzyme Inhib. Med. Chem.* **2002**, *17*, 227.
24. Dal Piaz, V.; Ciciani, G.; Chimichi, S. *Heterocycles* **1985**, *23*, 365.
25. Dal Piaz, V.; Ciciani, G.; Turco, G.; Giovannoni, M. P.; Miceli, M.; Pirisino, R.; Perretti, M. J. *J. Pharm. Sci.* **1991**, *80*, 1417.
26. Dal Piaz, V.; Giovannoni, M. P.; Castellana, M. C.; Palacios, J. M.; Beleta, J.; Domenech, T.; Segarra, V. *J. Med. Chem.* **1997**, *40*, 1417.
27. Dal Piaz, V.; Rascon, A.; Dubra, M. E.; Giovannoni, M. P.; Vergelli, C.; Castellana, M. C. *Il Farmaco* **2002**, *57*, 89.
28. Dal Piaz, V.; Vergelli, C.; Giovannoni, M. P.; Scheideler, M. A.; Petrone, G.; Zaratin, P. *Il Farmaco* **2003**, *58*, 1063.
29. Giovannoni, M. P.; Cesari, N.; Vergelli, C.; Graziano, A.; Biancalani, C.; Biagini, P.; Ghelardini, C.; Vivoli, E.; Dal Piaz, V. *J. Med. Chem.* **2007**, *50*, 3945.
30. Montesano, F.; Barlocco, D.; Dal Piaz, V.; Poggesi, E.; Fanelli, F.; De Benedetti, P. G. *Bioorg. Med. Chem.* **1998**, *6*, 925.
31. Renzi, G.; Pinazauti, S. *Il Farmaco Ed. Sci.* **1969**, 885.
32. Vergelli, C.; Giovannoni, M. P.; Pieretti, S.; Di Giannuario, A.; Dal Piaz, V.; Biagini, P.; Biancalani, C.; Graziano, A.; Cesari, N. *Bioorg. Med. Chem.* **2007**, *15*, 5563.
33. Ye, Z. C.; Sontheimer, H. *Cancer Res.* **1999**, *59*, 4383.
34. Magnusson, K. R. *Mech. Ageing Dev.* **1998**, *104*, 227.
35. Natale, N. R.; Szabon-Watola, M. I.; Twamley, B.; Bridges, R. J.; Patel, S.; Rajale, T. *Acta Crystallogr., Sect. E* **2009**, *65*, 0144.
36. Chen, G. Q.; Gouaux, E. *Proc. Nat. Acad. Sci. U.S.A.* **1997**, *94*, 13431.
37. Cheng, Y. C.; Prusoff, W. H. *Biochem. Pharmacol.* **1973**, *22*, 3099.
38. Dowd, L. A.; Coyle, A. J.; Rothstein, J. D.; Pritchett, D. B.; Robinson, M. B. *Mol. Pharmacol.* **1996**, *49*, 465.
39. Esslinger, C. S.; Agarwal, S.; Gerdes, J. M.; Wilson, P. A.; Davies, E. S.; Awes, A. N.; O'Brien, E.; Mavencamp, T.; Koch, H. P.; Poulsen, D. J.; Chamberlin, A. R.; Kavanaugh, M. P.; Bridges, R. J. *Neuropharmacology* **2005**, *49*, 850.
40. Mavencamp, T. L.; Rhoderick, J. F.; Bridges, R. J.; Esslinger, C. S. *Bioorg. Med. Chem.* **2008**, *16*, 7740.
41. Hunston, R.; Gerothanassis, I.; Lauterwein, J. *Org. Mag. Res.* **1982**, *18*, 120.
42. Edmonds, D. T.; Summers, C. P. *J. Mag. Res.* **1969**, *12*, 134.
43. Bridges, R.; Patel, S. In *Topics in Medicinal Chemistry*; Napier, S., Ed.; Springer: NY, 2009.
44. Sontheimer, H. *J. Neurochem.* **2008**, *105*, 287.
45. Burkhart, D. J.; Twamley, B.; Natale, N. R. *Tetrahedron Lett.* **2001**, *42*, 8415.
46. Szabon-Watola, M. I., Ph.D. Thesis, University of Idaho, 2006.
47. Martin, D. L.; Shain, W. *J. Biol. Chem.* **1979**, *254*, 7076.
48. Nicholls, D. G.; Sihra, T. S.; Sanches-Prieto, J. *J. Neurochem.* **1987**, *1987*, 50.
49. Vesce, S.; Bezzi, P.; Rossi, D.; Meldolesi, J.; Voltera, A. *FEBS Lett.* **1997**, *411*, 107.